NEURAL NETWORK MODELLING OF FORCES ON VERTICAL STRUCTURES

Marcel R.A. van Gent[1] and Henk F.P. van den Boogaard[1]

ABSTRACT: For the design of vertical breakwaters, reliable predictions of the horizontal forces are required. Through physical modelling useful predictions can be made but, due to the very complex interaction between waves and structures, the derivation of reliable empirical relations based on such tests can still be rather difficult. Here, based on a large data-set from physical model tests, use is made of Neural Network modelling to predict horizontal forces on vertical structures. In addition, a method is developed to estimate the reliability-intervals around the predictions. The resulting tool is a complementary design-tool for predicting forces on vertical breakwaters and also a suitable tool for application in probabilistic design methods.

1. INTRODUCTION

Horizontal forces on the upright seaward section of vertical structures often form the most important wave load. Due to the complexity of the phenomena, it is difficult to describe the effects of all relevant parameters in design formulae. For such processes in which the interrelationship of parameters is unclear while sufficient experimental data are available, Neural Network (NN) modelling may be a suitable alternative. Mase *et al.* (1995) showed that this technique is valuable for the stability analysis of rubble-mound breakwaters. Here, an NN is developed for predicting wave forces on vertical structures where nine different parameters are considered important as the main factors that determine the total horizontal force. First the parameters that were used to determine the horizontal forces are discussed.

---

1) WL | DELFT HYDRAULICS, P.O. Box 177, 2600 MH Delft, The Netherlands.

Then the actual development of the NN is described, followed by a comparison with traditional design formulae. In addition, a method to assess the reliability of the NN-predictions is prcsented. More detailed information concerning this paper can be found in Van Gent and Van den Boogaard (1998).

2. NEURAL NETWORK MODELLING

2.1 PARAMETERS INVOLVED IN FORCE PREDICTION

The total horizontal force on a vertical breakwater is the result of the interaction between the wave field, the foreshore and the structure itself. Here perpendicular wave attack is considered. In order to describe the wave field two parameters are applied: The significant wave height in deep water (H_s) and the corresponding peak wave period (T_p). The effect of the foreshore is described by the slope of the foreshore ($tan\ \theta$) and the water depth in front of the structure (h_s). The structure is characterised by the height of the vertical wall below and above the water level (h' and R_c), the water depth above the rubble-mound foundation (d), the width of the berm (B_b) and the shape of the superstructure (φ). Figure 1 shows the nine parameters on which the NN was based.

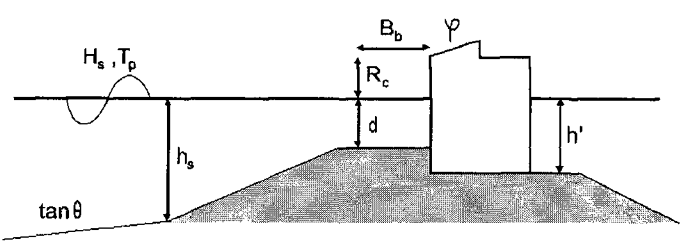

Fig. 1 Parameters used for NN-modelling of horizontal forces on vertical structures.

In particular, the crest shape factor (φ) was introduced to account for the differences in crest shapes of the structure, such as inclined or curved crests. Measured forces obtained under similar wave conditions and similar structures but with different crest shapes (vertical and non-vertical) were compared by computing the ratio of the corresponding horizontal forces. The average of the computed ratios was taken as the crest shape factor for that shape. The values were in the range from 0.8 to 1.0 (1.0 corresponds to a vertical crest). This approach was adopted in view of the fact that wave overtopping was not significant in those tests where the crest elements differ considerably from a simple rectangular caisson.

2.2 DESCRIPTION OF DATA-SET

Data on total horizontal forces on vertical structures are collected from physical-model tests performed at several laboratories. The applied measurement techniques and analysis methods differ from institute to institute. Based on published data the parameter corresponding to the total horizontal force that is exceeded by 99.6% of the waves has been derived. For some cases this parameter was not directly measured but has been obtained by interpolating between for instance the 99% and 99.8% values. For one data-set an extrapolation has been applied by using a Weibull-fit through the 90%, 95% and 98% values; the fit gave good predictions of the measured 99%-values and therefore has been applied to predict the corresponding 99.6% values. Nevertheless, inaccuracies may have been introduced by these interpolations and extrapolations.

The data is described in detail in the following publications: Van der Meer and Juhl (1992), Allsop et al (1996), Kortenhaus and Oumeraci (1997) and Madrigal and Wei (1997). In total 612 data-patterns have been used: 68 from DELFT HYDRAULICS (The Netherlands), 59 from DHI (Denmark), 97 from CEDEX (Spain), 215 from HR Wallingford (UK) and 173 from Leightweiss Institute (Germany).

As will be discussed, an analysis concerning the consistency of the data-set has been performed. It occurred that some data-sets, especially the relatively large data-sets, show significant variations in output for data-patterns with similar input-patterns. The inconsistencies in the data-set do not necessarily lead to incorrect predictions by the NN if these measurement errors can be considered as a random white noise, i.e. no 'systematic errors'.

One of the sources of inconsistencies in the data-set is that the data includes several types of wave forces. The data-set contains conditions that lead to pulsating wave forces but also conditions that lead to impact forces. Especially tests leading to impacts with a relatively low number of waves lead to relatively weak repeatability and therefore input-patterns with a less reliable output. However, if conditions are divided into classes of 'pulsating forces', 'impact forces' and 'transitional' according to the diagram by Kortenhaus and Oumeraci (1997), 244 patterns are identified as 'pulsating forces', 362 as 'impact forces' and 12 as 'transitional'. Inconsistencies such as large differences between output for similar input-patterns are not restricted to one of these classes (inconsistencies occur for 'impact forces' and for 'pulsating forces').

The accuracy of the NN-modelling depends strongly on the quality of the data-set. Therefore, for this application it is even of greater importance that a method is available to quantify the reliability of the NN-output. The consequence of the applied method is that the accuracy of the NN predictions can be further improved if more reliable data-patterns become available,.

2.3 NEURAL NETWORK TRAINING

General

Here, NN-modelling will be briefly discussed. For a more detailed but still general introduction a well written review on NN included in ACM (1994) is recommended, as well as the book of Beale and Jackson (1990). For further details on the technical background, examples, and applications the book of Haykin (1994) is very suitable.

NN can be seen as a sophisticated data-oriented modelling technique to find relations between input- and output-patterns without using process-knowledge. Here, the applied input-pattern is [H_s, T_p, $tan\theta$, h_s, h', R_c, d, φ, B_b] and the output is a single parameter [$F_{h\text{-}99.6\%}$]. For the preparation of an NN model a sufficiently large set of input-output patterns is required.

The configuration of an NN-model can vary. The NN is organised in the form of layers and within each layer there are one or more processing elements called 'neurons'. The first layer is the input layer and the number of neurons in this layer is equal to the number of input-parameters. The last layer is the output layer and the number of neurons in this layer is equal to the number of output parameters. The layers between the input and output layer are the so-called 'hidden layers'. Here, a configuration with only one hidden layer is chosen and information goes from the input-layer, via the hidden layer, to the output-layer ('feed-forward' configuration). Figure 2 shows an example of such a configuration.

Each neuron receives inputs from all neurons of the preceding layer via the connectivities. To each connectivity a weight is assigned. The total input of a neuron then consists of a weighted sum of the outputs of the preceding layer. The output of the neuron is generated using a 'non-linear activation function' with a sigmoid shaped form. This procedure is followed for each neuron; the output neuron generates the final prediction of the NN.

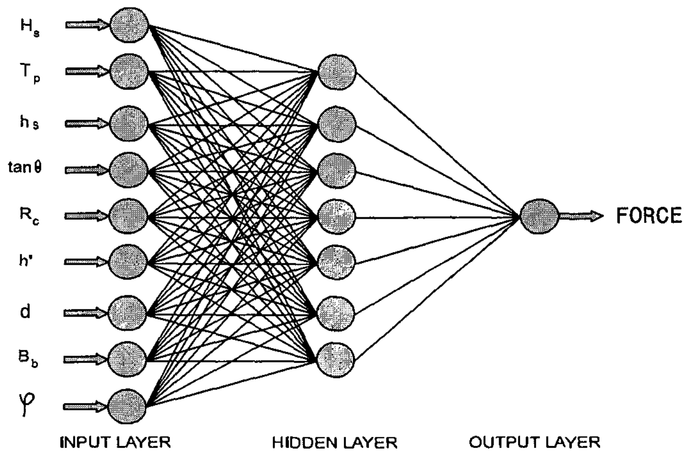

Fig. 2 NN-configuration.

Before the NN can be used the weight-factors need to be calibrated for which a part of the data-set is used (here: a 'training-set' of 500 of the 612 tests). This is the so-called 'training' of the NN using some 'learning' procedure. After that the NN need to be validated by using the remaining part of the data-set (here: a 'testing-set' of 112 of the 612 tests).

Training and testing

The calibration of the weight-factors is performed by using data for which both the input and the output are fed to the NN. Starting with an initial guess for the weights the procedure is that the inputs of this 'training-set' are fed to the NN and the NN's outputs are compared to the observed outputs (measured output). On the basis of the differences between both, the weights are adjusted in such a way that in the next step when the inputs are again fed to the NN, a better prediction is found. This procedure is repeated until no further improvements can be made. This iterative adjustment of the weights is called 'training' of the NN and usually this is done by minimisation of some cost function (or error function) that quantifies the differences of predicted outputs and the desired output (measured), often called 'targets'. A common form of cost function is a superposition of the squared differences. For the minimisation of the cost function, gradient based methods turn out to be most efficient and for the computation of gradient the well known 'error back propagation rule' is used. Here, for calibration the root-mean-square error is defined as:

$$RMS_{train} = \sqrt{\frac{1}{N_{train}} \sum_{n=1}^{N_{train}} \left(\left(F^{obs}_{H\text{-}0.4\%}\right)_n - \left(F^{NN}_{H\text{-}0.4\%}\right)_n \right)^2} \tag{1}$$

An important step in the NN-modelling is to find the optimal number of neurons in the hidden layer. By increasing the number of hidden neurons the differences between the NN-output and the desired output (measured) of the data used for calibration will decrease because more hidden neurons lead to more degrees of freedom (more weight-factors). However, there is a certain optimum because at a certain number of hidden neurons, the NN also starts to model 'noisy fluctuations' in the data-set which is unfavourable for the accuracy of the real predictions. At that moment the NN-model is 'overtrained'. To prevent such an overtraining of the NN not all available data is used for training; a part is reserved for verification. In this partition the 'training-set' and 'testing-set' must be equivalent in statistical sense (i.e. representative for the whole data-set). The optimal number of neurons can be found by training the NN for a range of numbers of neurons in the hidden layer and each time comparing the NN's performance (root-mean square error) on the training and testing-set. Figure 3 shows the performance of NN with various numbers of hidden neurons. More neurons lead to a better performance of the NN for the data used for training but at some stage the predictions of the remaining data (testing-set) become worse. This is an indication that at this stage, NNs with more hidden neurons are not suitable for generalisation and do not provide optimal predictions. This is shown in Figure 3 and in this case a configuration with 8 hidden neurons was chosen as the optimal NN.

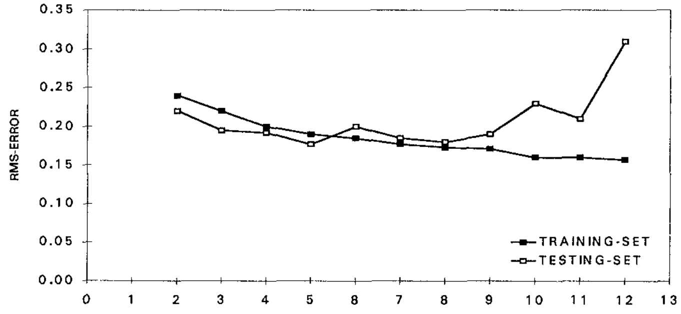

Fig. 3 *NN-performance with configurations with various numbers of neurons in hidden layer.*

Application

The aim of the NN is to be applied both for small-scale tests and for proto-type situations. Here the basic data-set is based on small-scale tests, however. Therefore a treatment to predict correct proto-type situations needs to be included. If for a certain input-pattern [H_s, T_p, $tan\theta$, h_s, h', R_c, d, φ, B_b] a prediction is required, this input-pattern is scaled by using the Froude-scaling law to an input-pattern with a wave height on which the NN is trained (here all patterns are scaled to a wave height of H_s=*0.1 m*). This also reduces the number input-parameters for the actual NN-configuration from 9 to 8 (here the configuration 8-8-1 is used which means 8 input parameters, 8 hidden neuron and 1 output parameter). The prediction by the NN ($F_{h-99.6\%}$) is then again scaled back to the actual wave height. This procedure where physical knowledge is incorporated in the NN, allows for predictions on different scales. However, this also introduces overpredictions for situations with wave impacts where the Froude-scaling law is not strictly valid.

Using the above described scaling of the data, the data-set can be statistically summarised as shown in Table 1. It must be taken into account that the input components of data-set are not uniformly distributed within the ranges of the parameters given in Table 1. This non-uniformity cannot be recognised from the univariate statistics of Table 1 and a more advanced approach must be followed to obtain an 'accurate' description of the input domain. This, as well as a method to obtain reliability-intervals for NN-predictions of the forces, will be addressed in the following section.

parameter	*mean*	*standard deviation*	*lower extreme*	*upper extreme*
H_s	*0.1*	*0.0*	*0.1*	*0.1*
T_p	*1.672*	*0.526*	*0.8208*	*4.208*
$tan\ \theta$	*0.0133*	*0.0090*	*0.0*	*0.025*
h_s	*0.300*	*0.147*	*0.046*	*0.8276*
h'	*0.206*	*0.110*	*0.0192*	*0.6557*
R_c	*0.221*	*0.136*	*0.0*	*0.8571*
d	*0.152*	*0.111*	*-0.0585*	*0.7000*
φ	*0.989*	*0.0387*	*0.8*	*1.0*
B_b	*0.221*	*0.224*	*0.0*	*1.221*

Table 1 *Statistical parameters of the scaled input-patterns of the data-set used for calibration/training.*

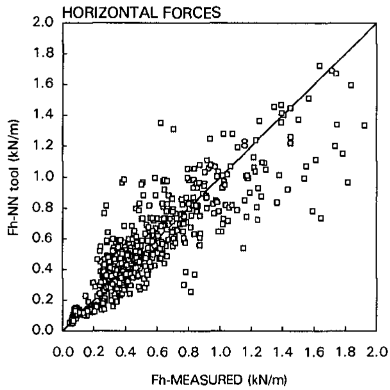

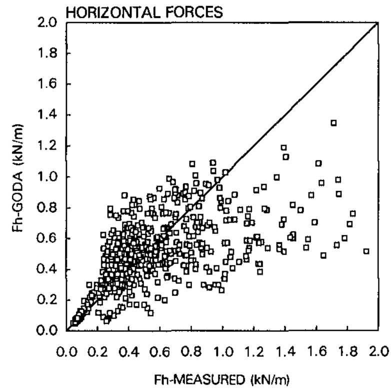

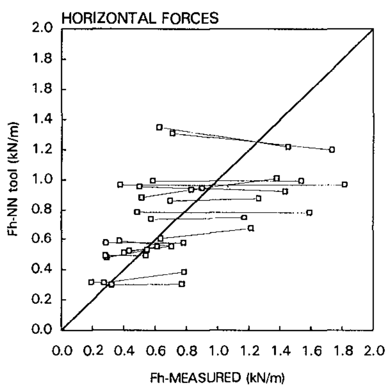

Fig.4 Comparison of measured and predicted (NN) horizontal forces.

Fig.5 Comparison of measured and predicted (Goda) horizontal forces.

Fig.6 Data-points with similar input but large differences in measured properties.

Fig.7 Comparison of measured and predicted (NN) horizontal forces (2 data-sets).

Fig.8 Comparison of measured and predicted (Goda) horizontal forces (2 data-sets).

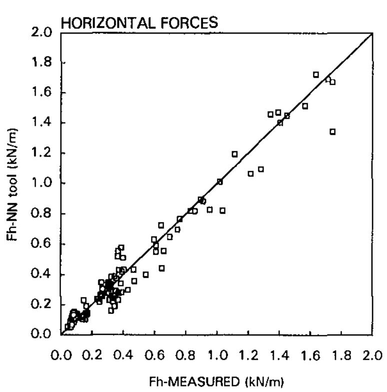

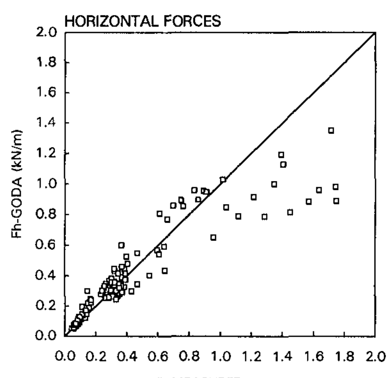

Comparison with Goda-method

Figure 4 shows a comparison between the measured horizontal forces and the predictions by the NN for all 612 data-patterns. Figure 5 shows a comparison between the same measured forces and the well-known Goda-method (Goda, 1985). For this data-set the scatter is large for both prediction methods. For this data-set the NN-output shows a better agreement than the Goda-method. The large scatter is not due to the prediction methods but mainly the result of inconsistencies in the data-set (see also Van Gent and Van den Boogaard, 1998).

In Figure 6 some data-patterns from Figure 4 which have the same, or nearly the same, input-pattern are connected with lines. This figure shows that for nearly identical input-patterns considerable deviations are observed in the measured output. For such input-patterns the NN-output shows nearly the same output, however this is consistent in contrast to the measured data which show rather large inconsistencies. Since the accuracy of the NN-predictions depends largely on the quality of the data-set, the observed inconsistencies in the data-set induce the necessity for information concerning the reliability of the NN-predictions. Although the NN is developed with data of all five data-sources, two data-sources do not show these inconsistencies. For those two data-sets Figure 7 and Figure 8 show the same comparison between measured data and predictions by the NN-tool and the Goda-method. The comparison between measured and by the NN-tool predicted forces shows a good agreement. For a relatively large part of the data-set, the Goda-method underpredicts the forces. The comparisons indicates that the NN-tool can serve as a complementary design-tool. In the following section, a method to quantify the reliability of the predictions is discussed.

3. RELIABILITY INTERVALS

Here, a tool is described to obtain reliability-intervals for the horizontal force predictions of the NN. Since the NN is calibrated with a data-set that does not uniformly cover all possible situations, the NN in fact interpolates between certain measured data-patterns or extrapolates from a region with measured data-patterns. The NN-tool, like other 'fit-procedures' is more suitable for interpolation than for extrapolation. The tool to quantify the reliability is based on information of the distribution of the data-set, hereafter the *training-set*, over the range of the parameter-domain covered by the measured parameter combinations. It is noted that the here developed approach is quite general and is not restricted to the NN-modelling of forces on vertical breakwaters (more details can be found in Van Gent and Van den Boogaard, 1998).

Three steps are distinguished in this approach: First it is studied how the input-parameters of the training-set are distributed over their domain; then a method is developed to decide whether or not a prediction by the NN can be accepted or not, and finally a method to quantify the reliability of an NN-prediction is described.

In the first step the parameter-domain spanned by the input-patterns of the training-set is determined by means of a probability density function (PDF) $f(\cdot)$. In particular the PDF can be used to determine which parts of the input parameter-domain are densely represented by the training-set (and where the NN will generate the most accurate predictions) and which parts are sparse, or even absent (and where the NN is used for extrapolation rather than interpolation).

Following the approach suggested by Van den Boogaard *et al* (1993) a very suitable and accurate way to find an estimate of the PDF $f(\cdot)$ is to place a basis function $\varphi(\cdot)$ at every input-pattern of the training-set and then take the superposition of all these basis functions. In this way the basis function $\varphi(\cdot)$ spreads each point over its neighbourhood and for this reason $\varphi(\cdot)$ is called a *Point Spread Function* (PSF). Often a (multivariate) Gaussian profile is chosen for the PSF and a copy of this Gaussian functions is centred at each input-pattern. Gaussian functions have (multivariate) ellipsoids as iso-lines and the form of these ellipsoids (i.e. the directions and lengths of the principal axes) is uniquely determined by the covariance matrix within the formula of a Gaussian function. For the PSF $\varphi(\cdot)$ this covariance matrix Σ_p cannot be chosen arbitrarily but must be derived from the N input-patterns within the training-set. This is done in such a way that the superposition of all the Gaussian Point Spread Functions provides the most accurate estimate of the PDF $f(\cdot)$. From the derivation of this 'optimal' covariance function it also follows that the PSF $\varphi(\cdot)$ is centred at 0. All this leads to:

$$f(\vec{x})=\frac{1}{N}\sum_{n=1}^{N}\varphi\left(\vec{x}-\vec{X}_n\right) \quad \text{with} \quad \varphi(\vec{\xi}):=\frac{1}{\left(\sqrt{2\pi}\right)^D\cdot\sqrt{|\Sigma_p|}}\exp\left[-\tfrac{1}{2}\vec{\xi}^T\cdot\Sigma_p^{-1}\cdot\vec{\xi}\right] \tag{2}$$

where D is the number of input-parameters (dimensions), N is the number of input-patterns, Σ_p is a covariance matrix, $\vec{X}_n$ denotes the n-th input-pattern, and $\vec{x}$ is the vector of the input-pattern for which the prediction by the NN is required. This provides the density-function for a certain input-pattern for which the NN is applied. If this density-function exceeds a certain minimal threshold value δ, one can say that the input-pattern is close to input-patterns of the training-set, and thus the NN can provide a relatively accurate result. The remaining problems are first to define a proper threshold-value δ for which the prediction of the NN can still be accepted and secondly, if a prediction can be made, to quantify the reliability of the predictions.

To illustrate the above described technique Figure 9 shows the principle for data with two parameters (x,y) only. The basic-data (i.e. the training-set) is non-uniformly spread over the parameter-domain. For predictions within the range of the basic-data (Data-point 1), a relatively reliable prediction will be obtained. For a prediction outside the range of the basic data the predictions are based on extrapolation and will be less reliable. When extrapolating in a direction with basic-data, a relatively reliable extrapolation might still be obtained (Data-point 3). For extrapolations in a direction with low spread, the reliability of the extrapolation (and thus the prediction of the NN) will be unreliable (Data-point 2) (ellipsoids in Figure 9 denote iso-lines of the PSF $\varphi(\cdot)$ centred at the measured input-patterns; the PDF $f(\cdot)$ is the superposition of these PSFs and provides the density of the input data-set).

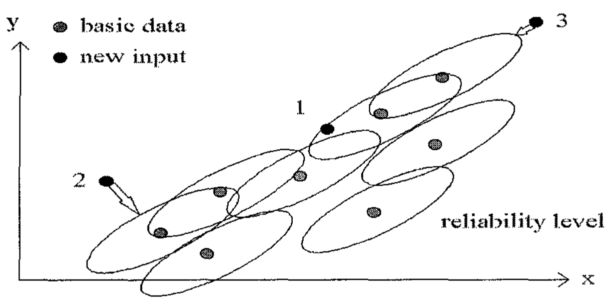

Fig. 9 Principle of applied technique for obtaining reliability intervals.

To obtain a proper threshold-value δ for which a prediction by the NN can be accepted, a 'level of significance α' is introduced. Then the PSF $\varphi(\cdot)$ is used to define an ellipsoid (forming an iso-line of the PSF) that is placed around the input-pattern $\vec{x}$ for which an NN-prediction is required. The 'radius' of this ellipsoid is R_α and it depends on the significance level α. R_α is such that the volume of the ellipsoid is a fraction $\beta := 1-\alpha$ of the total volume of the PSF. It can be shown that for a given α this radius must satisfy the equation $\gamma(\frac{1}{2}D, \frac{1}{2}R_\alpha^2) = 1-\alpha$ where $\gamma(\cdot,\cdot)$ is the incomplete gamma-function. The relation between the threshold-value δ and the radius R_α is then as follows:

$$\delta = \varphi(\xi_\alpha) = \frac{1}{N\left(\sqrt{2\pi}\right)^D \cdot \sqrt{|\Sigma_p|}} \exp\left[-\tfrac{1}{2} R_\alpha^2\right] \tag{3}$$

Then all input-patterns $\vec{X}_n$ of the training-set are selected that are within the ellipsoid of the radius R_α around the new input $\vec{x}$. These patterns of the training-set are used to derive the 95% reliability interval for the NN's prediction of the total horizontal force for the new input $\vec{x}$. The number of the so selected input-patterns depends on the value that is chosen for the significance level α. From a sensitivity analysis a value $\alpha=0.05$ turned out to be very suitable in practice. If no input-patterns of the training-set are within the ellipsoid, the corresponding NN-prediction will be considered as unreliable and no reliability-interval is defined. If a number of K input-patterns (with $K \geq 1$) of the training-set are within the ellipsoid, the reliability-interval around the prediction for the new input-pattern $\vec{x}$ is determined based on the measured outputs T_k ($F_{h\text{-}99.6\%}$) belonging to the input-patterns $\vec{X}_n$ within the ellipsoid. The mean and variance of the outputs of T_k can be estimated by:

$$\langle T_k \rangle = \frac{1}{K} \sum_{k=1}^{K} T_k \quad , \quad \sigma^2_{\langle T \rangle} = \frac{1}{K \cdot (K-1)} \sum_{k=1}^{K} \left(T_k - \langle T \rangle \right)^2 \tag{4}$$

Assuming that the mean of the K outputs satisfy a Gaussian distribution, the 95%-reliability-interval is:

$$\left(\langle T_k \rangle - 1.96 \cdot \sigma_{\langle T \rangle} \, , \, \langle T_k \rangle + 1.96 \cdot \sigma_{\langle T \rangle} \right) \tag{5}$$

The mean of the outputs $\langle T_k \rangle$ is in general not equal to the prediction by the NN. The reliability-interval however, is considered as a useful measure for the reliability of the prediction. Therefore, for the final reliability-interval around a prediction by the NN, i.e. $NN(\vec{x})$, the following measure is used:

$$\left(NN(\vec{x}) - 1.96 \cdot \sigma_{\langle T \rangle} \, , \, NN(\vec{x}) + 1.96 \cdot \sigma_{\langle T \rangle} \right) \tag{6}$$

Inaccurate test-results that are used for training the NN, such as those with observed inconsistencies leading to the relatively large scatter (Figure 4), affect the prediction of the NN but this also leads to a wider reliability-interval around the prediction. This justifies that also these tests are used for the NN; the user of the NN-tool is given a prediction but in regions with relatively unreliable basic-data, this prediction will involve a wider reliability-interval.

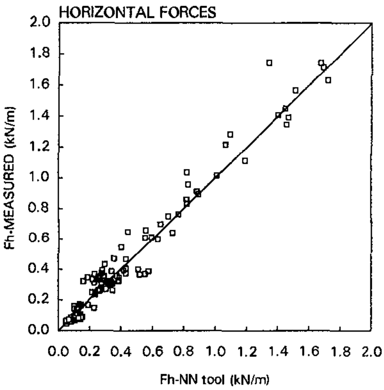

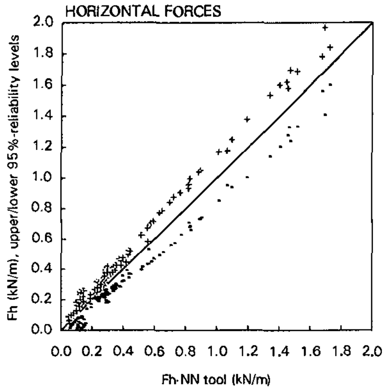

Fig. 10 Predictions by NN-tool (left) and reliability-intervals (right).

As an example of the above described approach the predictions by the NN-tool are shown in the left graph of Figure 10 (as in Figure 7) while the right graph shows the upper limits and the lower limits of the 95%-reliability-intervals for these predictions. This approach which yields insight in the accuracy of the predictions prevents application of the NN for situations where no basic-data is available (significant extrapolation) and also provides a measure for the reliability of the predictions for situations where sufficient tests in the applied data-set are available.

4. CONCLUSIONS

The presented results show that Neural Network modelling can well be used for the prediction of horizontal forces on vertical structures. A tool has been developed to obtain a reliability-interval for the Neural Network predictions. Still, the accuracy of the Neural Network is largely determined by the quality of the data-set. It has been shown that the differences between the Neural Network predictions and the measured values are to a large extend caused by inconsistencies in the data-set. For the data-sets that show none of the observed inconsistencies the comparison between the NN-output and the measured forces is good and the agreement is such that the tool can be used as a complementary design tool. For the present data-set the predictions by the NN-tool show a better comparison with the measured data than the Goda-method.

ACKNOWLEDGEMENTS

This study was co-sponsored by the Commission of the European Communities within the framework of the MAST-PROVERBS project (contract MAS3-CT95-0041). Mr. M.D. Sánchez (IHE/DELFT HYDRAULICS) is acknowledged for his preliminary study which led to valuable insight in applications of NN-modelling for the present subject.

REFERENCES

ACM (1994), *Communications of the ACM: Artificial Intelligence*, Volume 37, Number 3, March 1994.

Allsop, N.W.H., D. Vicinanza and J.E. McKenna (1996), *Forces on vertical breakwaters and related structures*, Research report SR443, HR Wallingford, (revised version).

Beale, R,, T. Jackson (1992), *Neural Computing: An Introduction*, Institute of Physics Publishing Ltd, London.

Goda, Y. (1985), *Random seas and design of maritime structures*, University of Tokyo Press, Tokyo.

Haykin, S. (1994), *Neural Networks. A comprehensive Foundation*, Macmillan College Publishing Company, New York, 1994.

Kortenhaus, A and H. Oumeraci (1997), *Supplementary data for response map*, MAST-PROVERBS proceedings, Overall workshop 18-22 February 1997, Las Palmas, Spain.

Kreyszig, E. (1970), *Introductory Mathematical Statistics. Principles and Methods*, Wiley&Sons, New York.

Madrigal, B.G. and C. Wei (1997), *Analysis of pressure measurements on composite breakwater from 2D tank tests performed during the MCS-Project, MAST-II*, MAST-PROVERBS proceedings, Overall workshop 18-22 February 1997, Las Palmas, Spain.

Mase, H., Sakamoto, M. and Sakai, T. (1995), *Neural network for stability analysis of rubble-mound breakwaters*, J. of Waterway, Port, Coastal and Ocean Engrg, ASCE, nov/dec 1995, pp. 294-299.

Van den Boogaard, H.F.P, M.J.J. Hoogkamer, and A.W. Heemink (1993), *Parameter identification in particle models. Stochastic Hydrology and Hydraulics*, Vol. 7, No. 2, pp. 109-130.

Van der Meer, J.W. and J. Juhl (1992), *Quasi-static wave forces on vertical structures, re-analysis of data at the Danish Hydraulic Institute and Delft Hydraulics*, Project Report 2, prepared for MAST G6-S Coastal Structures.

Van Gent, M.R.A. and H.F.P. van den Boogaard (1998), *Neural network and numerical modelling of forces on vertical structures*, Proc. of 2nd Overall Project Workshop MAST-PROVERBS, Chapter 1.9, February-1998, Naples.

Pore pressures in vertical breakwater foundations

C. Zwanenburg[1]
M.B. de Groot[1]
T.J. Kvalstad[2]
A. van Hoven[1]

Abstract

When calculating the stability of a breakwater foundation information on the pore pressures directly underneath the caisson in the bedding layer and in the sand layer is needed. In this paper easy to handle calculation techniques are presented to derive the pore pressures underneath the caisson. A quasi-stationary calculation technique has been verified for the situation of a caisson breakwater, by a hindcast of laboratory tests. The differences between the quasi-stationary calculations and the laboratory measurements appear to be small and can be explained by non-stationary effects. The pore pressure distribution in real cases may considerably deviate from the traditionally assumed triangular distribution, due to several effects. Non-stationary effects are only relevant if the rubble is relatively fine and wave impact occurs. The pore pressures in the sand layer have been studied by centrifuge tests. Two types of pore pressure development can be distinguished, the instantaneous pore pressures, which follow the wave action at sea and the residual pore pressures, which gradually develop under repetition of loading. The residual pore pressures may lead to liquefaction if silt or fine sand is present in the subsoil.

Introduction

In the past many vertical breakwaters have been built. Several have been collapsed or suffered severe damage, see [Oumeraci, 1994]. When judging the stability of the foundation of a vertical breakwater the strength of the subsoil is important. Until recently only little was known about the strength of the vertical breakwater foundation and the strength development during wave attack. In this paper a study on the influence of the pore pressures on the strength of the rubble mound and the subsoil is presented.

[1] Delft Geotechnics, Stieltjesweg 2 P.O. Box 69 2600 AB DELFT, The Netherlands
[2] Norwegian Geotechnical Institute, P.O. Box 3930 Ullevaal Hageby N-0806 OSLO, Norway

In the following only vertical, caisson breakwaters are considered. The results, however, can also be applied to block walls. The caissons are assumed to be placed on a rubble mound. Underneath the rubble the original subsoil is present. Pore pressures in the subsoil will only be explicitly predicted if the subsoil consists of sandy material.

The water pressures in the rubble and in the subsoil, in the following referred to as pore pressures, are fluctuating by the wave action at sea. The pore pressures fluctuate around an average pressure level, corresponding to mean sea level. The wave-induced deviations in pore pressures are referred to as excess pore pressures. So the actual pore pressures are a summation of the average pore pressures and the excess pore pressures. In this paper only the excess pore pressures will be discussed. The resultant of these pressures along the caisson bottom is referred to as uplift force.

The total stress in the rubble and the subsoil consists of two components the pore pressure and the effective stress. When the total stress remains constant and the pore pressure increases as a result of wave action the normal effective stress decreases and the shear resistance, being the product of normal effective stress and the tangent of the friction angle, decreases proportionally.

Three main failure modes of a caisson foundation can be distinguished:

- Sliding over the foundation
- Bearing capacity failure of the rubble
- Bearing capacity failure of the subsoil

The three failure modes are depicted in figure 1. In reality a number of combinations of the above mentioned failure modes can be observed. In all the failure modes the pore pressures play an important role. They determine the uplift force relevant for the first mode, the reduction of the shear resistance in the mound, relevant for the second mode and the reduction of the shear resistance in the subsoil relevant for the last mode.

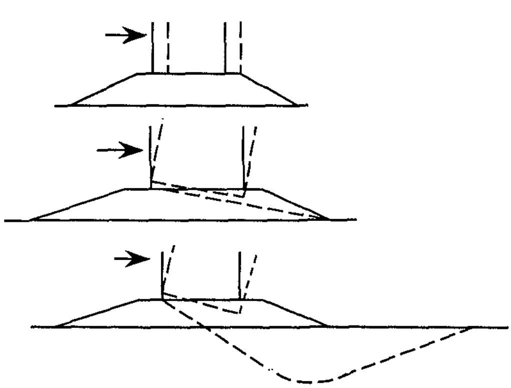

Figure 1 Failure modcs

Pore pressures in rubble

Linear pressure distribution

Traditionally, the pore pressures along the caisson bottom are estimated by a triangular shaped distribution. The water pressure at the front edge of the caisson bottom can be calculated by an analytical equation, e.q. the Goda formula. Since at the harbour side of the caisson no wave action is assumed to be present, the excess pore pressures at the harbour side toe of the rubble are negligible. Linear interpolation between the two points leads to the previous mentioned triangular shaped water pressure distribution underneath the caisson bottom.

Validation of a stationary numerical model

The linear pressure distribution is valid for a homogeneous bedding layer with a constant small thickness. When considering other cases a more sophisticated model is needed. In soil mechanics laminar flow models are used to simulate a stationary ground water flow situation. These models are based on Darcy's law in combination of the continuity equation. When applying these equations, only the permeability and the layout of the rubble and subsoil need to prescribed. This limited amount of information makes these models easy to be used.

These models however imply a number of restrictions.

- Stationary flow: the non-stationary effects will be discussed below
- Laminar flow: in coarse rubble the flow will usually be turbulent, however, corrections can be made by an adaptation of the permeability distribution.
- Incompressible water: this not a serious restriction for this situation.

The validity of the application of such a model (MSEEP) for calculating the pore pressure development in the rubble layer underneath a caisson is studied with a hindcast of large-scale laboratory tests.

The laboratory tests have been carried in the large wave flume of Hannover, see [Kortenhaus et el, 1994]. In this wave flume a test caisson has been constructed. The caisson height was about 2,76 m and the caisson width 3.0 m. The caisson was placed on a rubble mound with a thickness underneath the caisson of 0.60 m, a height at the front of 1.02 m and 0.77 m at the backside. Below the mound and separated by a geotextile a sand layer with a thickness of about 2 m was present. This sand layer was placed on the concrete floor of the flume.

The water pressures have been measured at several locations in the model. Directly underneath the caisson 6 rows of pore pressure transducers were located. The first row on top of the rubble, directly below the caisson bottom. The next row in the middle of the rubble layer. The following rows were located in the sand layer.

Four water pressure transducers have been placed in the front slope of the rubble. The readings of these transducers are used to determine the boundary conditions for the numerical model calculations. The pressures measured underneath the caisson are used to validate the calculation results.

A large number of waves have been applied on the test model. Two regular waves have been selected for this hindcast. First a smooth non-breaking wave, $H = 0.7$ m and $T_p = 6.5$ s, has been selected, secondly a breaking wave including wave impacts, $H = 0.9$ m and $T_p = 3.5$ s. Despite differences in wave characteristics, the maximum wave induced pressures in the rubble at the front of the caisson were nearly equal for both waves.

For the validation of the quasi-stationary calculation technique four moments in time have been selected from the continuously measured time-series. The moments are indicated by the water level at the front of the caisson:

- wave crest
- falling water level, passing still water level
- wave trough
- rising water level, passing still water level

The exact moments in time are selected from the reading of the pore pressure transducer, closest to the caisson front.

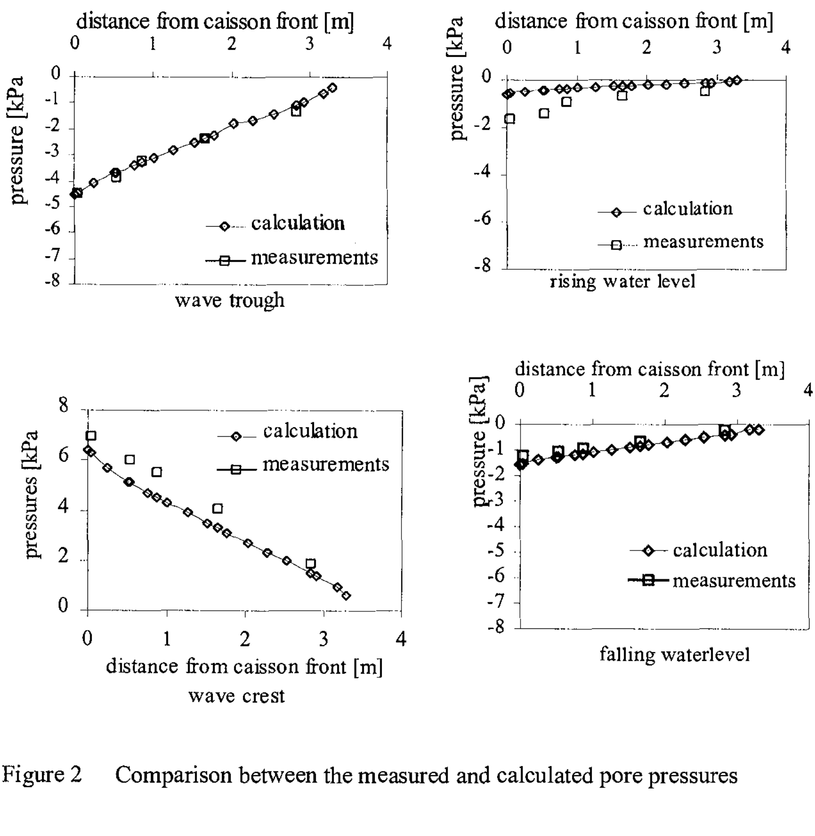

Figure 2 Comparison between the measured and calculated pore pressures

In figure 2 the validation results for the breaking wave are presented for each of the four conditions. From these graphs the following can be notified:

- Differences between the measured and calculated pore pressures in the rubble are found to be negligible for wave trough conditions.
- Differences are found for the situation at which the water level at the front passes still water level. For the rising water level more difference is found then for the falling water level.
- For the wave crest differences up to 20 % are found.

The calculations of the non-breaking wave show similar tendencies. Except that the differences for the wave crest are negligible, like for the wave trough.

Non-stationary effects can explain the differences between the measured and calculated pore pressures for the rising and the falling water level. When the water level passes still water level, the acceleration of the water flow reaches it's peak value and the time-depending effects of inertia and elastic storage become important.

The differences in pore pressures found for the wave crest with its temporarily high peak forces during the wave impact can also be explained by non-stationary effects, as will be discussed below.

In the scale model a homogeneous rubble layer with constant thickness has been applied. Consequently, an almost triangular shaped distribution is found for the wave crest as well as for the wave trough.

Stationary model applied in practice

No triangular pressure distribution is found, however, if the grainsize distribution of the rubble is non-homogeneous. When at one side of the caisson finer material is used more flow resistance and larger pore pressure gradients are found in the region of the finer material. An example is presented in figure 3. That such a pore pressure distribution may be realistic was demonstrated by measurements underneath the Porto Torres breakwater [Franco, 1996].

Not only the deviation in grainsize distribution leads to a deviation of the triangular shaped pore pressure distribution underneath the caisson. Other causes for deviation from the linear distribution may be:

- All kinds of natural activities, like animals or plants, may block the pores in the rubble. This leads to a gradual reduction of the permeability of the rubble.
- The presence of impermeable, tightly placed apron slabs in front of the breakwater.
- Flow concentration around the edges in combination with the effect of turbulence, especially with high mounds.
- When the caisson bottom does not connect perfectly to the top of the rubble some space is present larger then the average pore volume.

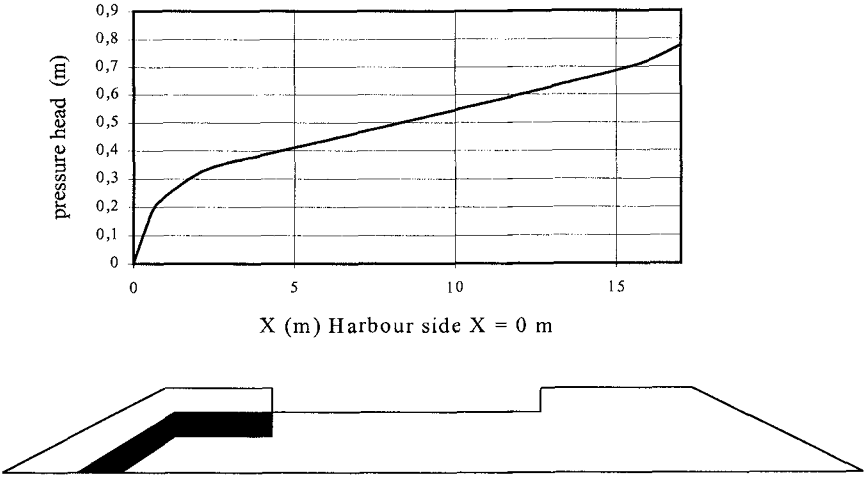

Figure 3 Pressure head distribution along the caisson floor at wave crest with non-homogeneous rubble (black represents fines of quarry run at harbourside)

Non-stationary effects

The quasi-stationary calculations approximate the actual pressures until a certain level of accuracy. For a more accurate approximation of the pressures the non-stationary effects need to be included.

In this study it is assumed that the non-stationary effects can simply be added to the results of the quasi-stationary calculations. Furthermore the non-stationary effects are split into two different components. First the effect of the (pressure) wave passing the caisson foundation is studied. For this situation the caisson is assumed to be completely fixed. This is referred to as the direct component. The second component is the indirect component. For this situation the movement of the caisson is studied independently from the wave action at sea. The water level at the front of the caisson is assumed at still water level. The excess pore pressures underneath the caisson are caused by the rocking and uplift motions of the caisson. Both components are presented in figure 4. In the following it is assumed that these phenomena can be studied individually from each other and that superposition of these components is allowed.

The non-stationary effects will be discussed for the situation of wave crest with wave impact, as this is the most relevant situation for the stability of the foundation.

Direct component

The first approximation of the direct component is a quasi-stationary pore pressure distribution, as can be found from the numerical calculations. According to this approximation all pore pressure-time curves in the bedding layer would have the same shape as the pressure-time curve at the front of the caisson and the variations would also be simultaneous. All pressures need only be reduced with a factor, which is constant for each location and can be found from quasi-stationary calculations or, even more simplified, with a linear distribution, as proposed by Goda and many others.

Inertia and elastic compressibility, however, influence the direct component during wave impacts with short duration: the pressure wave induced at the seaside needs some time to pass through the bedding layer. The combination of inertia, elastic compressibility in the two phases (soil skeleton and water, which is compressible due to small air bubbles) makes analytical solutions rather complicated. Before trying to find such analytical solution, two approximations of the direct component are presented:

- Approximation for one-phase material: "acoustical wave"
- Approximation without inertia: "elastic storage".

Both approximations will be studied in the next sections in order to find formulations for the relevant corrections to the quasi-stationary approach.

Acoustical wave in direct component

The propagation of the wave impact pressure variation through the rubble mound can be described as an acoustical wave if inertia and compression of the rubble-water mixture are modelled and

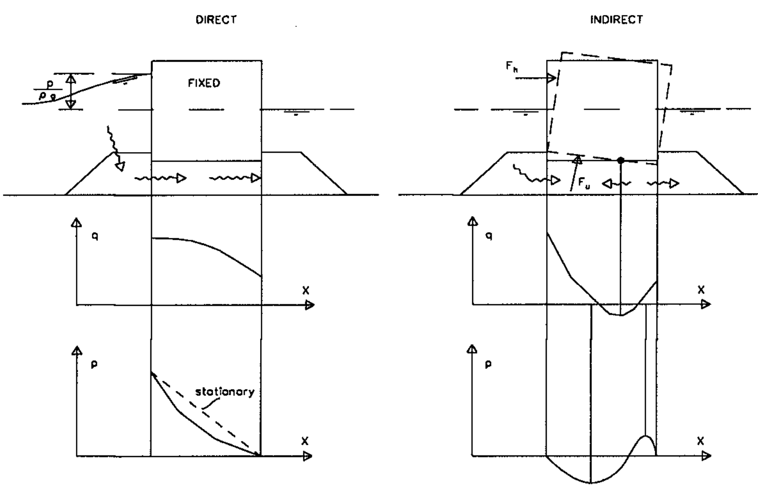

Figure 4 Distinction between direct and indirect component

if the mixture can be considered as a one-phase material. Last condition is met either if both phases move together ("no drainage"), as occurs with fine grained material, or if the water phase moves alone, hardly hindered by the rubble ("complete drainage"), as occurs with very coarse rubble.

Equations for both cases have been developed [MAST III / PROVERBS 1999] in order to quantify the influence on the uplift force during wave crest. This influence depends on the duration of the wave impact, the width of the caisson and the stiffness of the rubble skeleton and pore water. A maximum increase of the uplift force of 30 %, of the static situation, may only occur if the duration and stiffness are very small, where as the width is very large. Otherwise, the influence is negligible.

Elastic storage in direct component

According to the assumption used for the "acoustical wave", no energy loss, thus no damping occurs with the acoustical wave transmitted through the mound. For the completely undrained case it is assumed that the pore pressure variation at the seaside is transferred from the water to the skeleton without relative movement of the water through the skeleton. For the completely drained case, it is assumed that the fluid moves freely through the skeleton, without any stress transfer ("friction") to the skeleton. Both extremes are rather unlikely with the grainsizes usually applied in a mound.

There will be some relative movement of the water with respect to the skeleton together with friction and, consequently, energy loss. This effect in combination with the compression of the water, but without inertia, can be modelled with the one dimensional storage equation for elastic compression of the pore water.

The solutions of this equation yield an equation for the characteristic length for elastic storage, L_{esp}, a function of impact duration, pore water stiffness and permeability of the rubble, [MAST III/ PROVERBS, 1999]. This characteristic length should be compared with the caisson width, B_c. The characteristic length can be determined with equation 1.

$$L_{esp} = \sqrt{\frac{Tc_v}{\pi}} \tag{1}$$

Where;

$$c_v = \frac{k \times K_w}{n\gamma_w}$$

T	= wave period
c_v	= consolidation coefficient
k	= permeability
K_w	= compressibility of the pore water
n	= porosity
γ_w	= unit weight of water

The progress is now largely determined by the parameter L_{esp}. If $L_{esp} >> B_C$ the elastic storage is not relevant and the pore pressure distribution may be quasi-stationary. With $L_{esp} < B_C$, the uplift force, $F_{u,max}$, will be reduced, as illustrated in figure 4.

Indirect component

The effect of the indirect component can be found by considering the case where the "external" forces, together with caisson inertia, cause uplift and rotation of the caisson, whereas the pressure heads at both outer ends of the caisson remain equal to the mean sea level, defined to be zero. (right hand side of figure 4).

The "external" forces are F_h and F_u. Where F_u is the resultant of the excess pore pressures along the caisson floor. In this case, however, these pore pressures are not considered explicitly. The pore pressures found below, are those which should be added to the quasi-stationary pore pressures to find the final value of F_u.

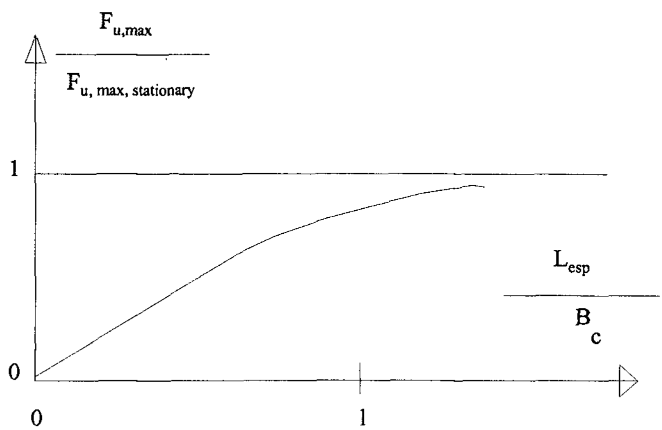

Figure 5 Influence of elastic storage on uplift force

Uplift causes an increase in pore volume; rotation causes an increase and a decrease in pore volume. Uplift and rotation together cause a change in pore volume, which is linearly distributed in x-direction, as illustrated at the right hand part of figure 4. The mass balance requires a flow velocity q, which will vary more or less parabolically in x-direction. This flow causes friction resistance, which is compensated by a pressure head gradient to meet the impulse balance. With the given zero pressure head at both ends of the caisson, a pore pressure decrease where the caisson rises and an increase where it descends.
An analytical equation has been developed to estimate the influence of the indirect effect [MAST III/ PROVERBS, 1999], i.e. the reduction of the uplift force during wave crest. Relevant parameters appear to be the impact duration, the caisson width, the skeleton stiffness and the permeability. The reduction appears to be significant for short impact duration, large caisson width, small skeleton stiffness and low permeability. Usually this is not the case.

By extended Finite Element calculations the effects of direct and indirect component have been studied separately, in the framework of the hindcast of the above mentioned large-scale tests in Hannover. For the calculations in which the caisson was completely fixed the calculated pore pressures did not differ from the pore pressures calculated for the free moving caisson. From these results the indirect component is considered of minor importance during these tests.

Pore pressures in the sandy subsoil

The influence of the wave action on the pore pressure development is among other things studied by centrifuge tests [van der Poel and de Groot, 1998]. These tests were carried out in the centrifuge of Delft Geotechnics in Delft. For these tests the 13 m (prototype) wide caisson was directly placed on the sand layer. The model was enclosed by a gravel layer, which covered the sandy subsoil. A lay-out of the prototype caisson is presented in figure 6. The figure shows two displacement meters on top of the model. Below the caisson pore pressure transducers were placed. First a row is placed in the caisson floor. Secondly a row of pore pressure transducers was placed at 2,70 m, prototype measures, below the bottom of the caisson.

A typical reading of the transducer indicated in figure 6 by a circle is presented in figure 7. From this figure two types of pore pressure development can be distinguished.

First type is the instantaneous pore pressures. These pore pressures follow the wave action at sea directly. This type of pore pressure development can be distinguished from the reading by the sharp high rise peaks.

The instantaneous pore pressures are caused by the deformation of the skeleton of the sand layer. The movements of the caisson cause compression, decompression and shear deformation of the skeleton of the sandy subsoil. At locations where compression occurs the pore volume decreases, leading to an increase of the pore pressures. At locations of decompression and shear deformation the pore volume increases, leading to a decrease of pore pressures. These fluctuations occur rapidly in time. For this reason the instantaneous pore pressures are hardly influenced by drainage effects. Only in a small top layer some drainage influences the pore pressures.

The second type of pore pressure development, the residual pore pressures, can be distinguished from the reading. These pore pressures induce a gradual increase of average pore pressure. Under a repetition of loading, the wave attack, the grains of the sand layer will show a tendency of re-arrangement. For many situations the subsoil will densify or show the tendency of densification. For these conditions the pore volume will decrease. This pore volume decrease leads to extra pore pressures. When by consolidation the excess pore pressures can not be completely drained off during the passage of one wave some residual pore pressures are left leading to an increase of average pore pressures.

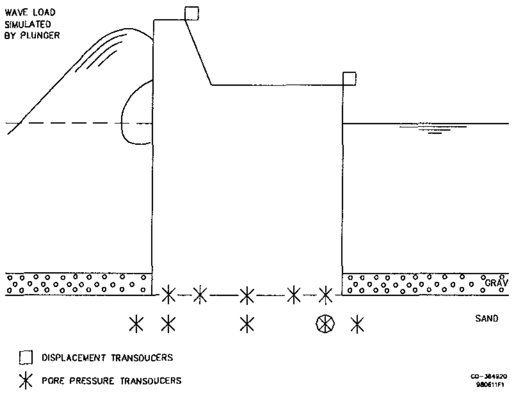

Figure 6 Model lay-out

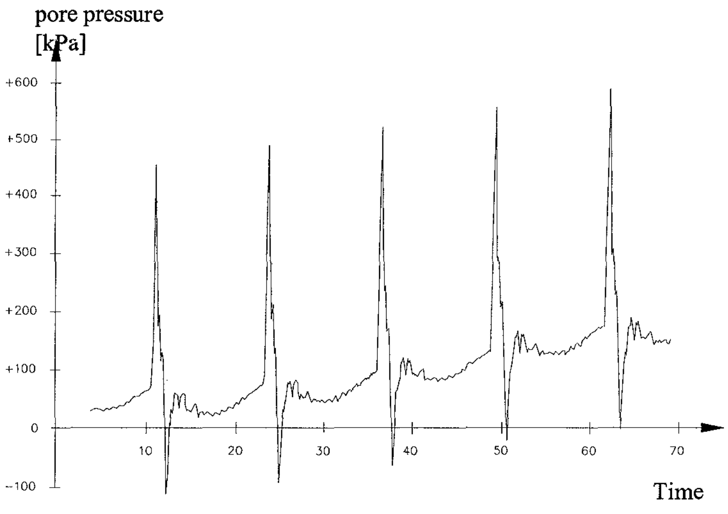

Figure 7 Pore pressure development

When full drainage occurs during a wave train or during a storm, the subsoil will densify and even the residual pore pressures will not remain. This might lead to deformations of the subsoil and to settlements at the surface. Where no drainage occurs the pore pressures will increase. A continuous increase of pore pressures will lead to liquefaction of the sandy subsoil. To judge whether this increase might lead to liquefaction the following rule of thumb is presented. When drainage period $T_{drainage}$

is smaller than 100 times the wave period T no significant pore pressure can be expected. When drainage period is longer the possibility of liquefaction should be considered. The parameter $T_{drainage}$ is a function of caisson width B_c and consolidation coefficient of the subsoil c_v.

$$\frac{T_{drainage}}{T} < 100 \qquad (2)$$

Where $$T_{drainage} = \frac{B_c^2}{c_v}$$

Application to a practical example

The above presented theories and equations have been applied to real existing structures. In this paper the results of the calculations for the breakwater Genoa Voltri, Italy, are presented.

The breakwater is located on a rubble layer with a thickness of up to 15 m. Below this rubble several soil layers can be distinguished. On top there is a silt layer with a thickness of 13 m. Below the silt layer there is a sand layer of 8.5 m of thickness. Underneath the sand layer there is a stiff clay layer with a strongly variable thickness. For the calculations a thickness of 9.5 m is applied. These soil layers are based on a rock foundation. The characteristic soil parameters are presented in table 1.

material type	unit weight	angle of internal friction	undrained shear strength	thickness of layer
	γ [kN/m^3]	φ [°]	c_u [kPa]	D [m]
Rubble	20	38	-	15
Silt	18.05	25-30	variable	13
Sand	19.62	29-35	variable	8.5
Clay	18.64	-	450	9.5

Table 1 Applied soil parameters

The following wave characteristics are applied

- significant wave height 8.3 m
- design wave height 13.2 m
- wave period 11.5 s

First the influence of the non-stationary effects are considered. For the acoustical wave approach it is found that the influence of these effects on the uplift force are negligible.

For the elastic storage approach L_{esp}/B_c is found to be equal to 4. From figure 5 it can be seen that for the elastic storage approach the uplift force equals to the stationary found uplift force.

Also the influence of the indirect component of the non-stationary effects appeared to be of minor importance.

From both simulations it can be concluded that the non-stationary effects are not relevant for the Genoa situation. The uplift force during wave crest can be calculated by stationary calculation techniques.

For the pore pressures in the subsoil the possibility of occurrence of liquefaction can be judged according to the equation 2. The results are presented in table 2.

	c_v	$T_{drainage}$	$T_{drainage}/T$
	[m²/s]	[s]	[-]
sand	1	506	44
silt	0.01	50 600	4 360

Table 2 Results of liquefaction judgement

For the sand layer the drainage period is short enough to prevent the occurrence of liquefaction. For the silt layer however it is possible for liquefaction to occur. For designing purposes for this situation a study focussed on liquefaction needs to be carried out.

With this information the stability can be calculated. Applying the stationary pore pressure distribution underneath the caisson in the rubble the factor of safety can be calculated for each of the earlier mentioned failure modes. The following safety factor are found:

- Sliding over the foundation $\mu = 1.73$
- Bearing capacity failure in the rubble $\mu = 1.27$
- Bearing capacity failure of the subsoil $\mu = 1.16$

According to the calculations the bearing capacity failure of the subsoil is the dominant failure mode. Sliding of the caisson over the rubble is found to be unlikely.

Conclusions

Pore pressures influence the stability of breakwater foundation. For preliminary design an easy to handle stationary flow model can be used to calculate the pore pressure underneath the caisson. Uneven distribution of the grain sizes in the rubble, a non-flat seabed and apron slabs may cause a significant deviation from the traditionally assumed triangular pressure distribution. To estimate the importance of non-stationary effects analytical equations and graphs can be used. The residual pore pressures in the sandy subsoil might lead to liquefaction if the drainage period is 100 times smaller then the wave period, which may be the case with silt or fine sand in the subsoil.

Acknowledgements

This study is performed in the framework of the MAST III / PROVERBS project, under joint funding of the European Union, The Dutch government (Rijkswaterstaat), Delft Geotechnics and the Norwegian Geotechnical Institute.

References

de Groot, M.B., K.H. Andersen, H.F. Burcharth, L.B. Ibsen, A. Kortenhaus, H.Lundgren, W. Magda, H. Oumeraci, W. Richwien, (1996). Foundation design of caisson breakwaters.

Franco, L. (1996). Analysis on of wave pressure measurements on plain and perforated caisson at Porto Torres Breakweter. MAST III/ PROVERBS, Las Palmas 1997.

van Hoven, A. (1998).Hindcast of pore pressures underneath Porto Torres breakwater van Hoven A., MAST III / Technical University Delft, Faculty of Civil Engineering and Delft Geotechnics CO-364920

Kortenhaus A., Oumeraci H., Kohlhase S., Klammer P. (1994).Wave –induced uplift loading of caisson breakwaters, ICCE '94, Kobe Chapter 94, pp 1297-1131

MAST III/PROVERBS (1999). Final report, Geotechnical Aspects, Volume IIb Leichtweiss institute, Technical University Braunsweig Germany 1999

Oumeraci H., (1994) Review and analysis of vertical breakwater failures and lessons learned. Coastal Engineering, volume 22 January 1994, ISSN 0378-3839.

van der Poel, J.T. and de Groot, M.B. (1998). Cyclic load tests on a caisson breakwater placed on sand. Centrifuge 98.